ACCSCIENCE PUBLISHING

Asian Journal of Water, Environment and Pollution

ORIGINAL RESEARCH ARTICLE

Land cover change and dry-season thermal patterns across the urbanizing areas in southeastern Vietnam

Nguyen Anh Tho[1,2†], Le Nguyen Hoa Tien[1,2†], and Tran Xuan Dung[1,2†*]

[1]Department of Oceanology, Meteorology and Hydrology, Faculty of Physics and Engineering Physics, University of Science, Ho Chi Minh City, Vietnam

[2]Viet Nam National University Ho Chi Minh City, Ho Chi Minh City, Vietnam

Abstract

Industrial urbanization is altering land cover and surface thermal conditions in southeastern Vietnam, but comparisons among secondary urban areas remain limited. This study compares impervious-surface expansion, vegetation indices, and February land surface temperature (LST) in selected urban areas of Binh Duong, Tay Ninh, and Binh Phuoc from 1999–2024. Eight Landsat scenes acquired in February between 1999 and 2024 were selected, comprising four Landsat 5 Thematic Mapper scenes and four Landsat 8 Operational Land Imager and Thermal Infrared Sensor scenes. Maximum likelihood classification was used to map land cover, while sensor-specific radiometric calibration and normalized difference vegetation index (NDVI)-based emissivity correction, using fixed NDVI endpoints of 0.2 and 0.5, were used to determine LST. Endpoint area statistics were subsequently calculated. Impervious area increased from 1,981 to 31,862 ha in Binh Duong, from 373 to 6,783 ha in Tay Ninh, and from 291 to 3,333 ha in Binh Phuoc. Endpoint-average net gains were 1,195, 256, and 122 ha per year. In 2024, mapped LST above 34 °C occupied 8,857, 81, and 348 ha in Binh Duong, Tay Ninh, and Binh Phuoc, respectively. Normalizing by the stated study extents yields high-temperature area shares of 8.91%, 0.32%, and 4.03%, distinguishing absolute high-temperature area from its relative coverage within each study mask. Land with NDVI > 0.4 covered 48,585, 18,802, and 6,593 ha, but these threshold areas are not equivalent to mutually exclusive vegetated land-cover classes. The results suggest contrasting corridor-led and clustered development patterns, and identify locations for further thermal assessment. Incomplete independent validation and unresolved atmospheric and emissivity uncertainties limit causal attribution and absolute-temperature interpretation. The comparison serves as a dry-season surface diagnostic rather than a continuous climatic trend or a measure of human heat exposure.

Keywords: Urban expansion; Landsat; Land surface temperature; Land cover; Southeastern Vietnam

†*These authors contributed equally to this work.*

***Corresponding author:**
Tran Xuan Dung
(txdung@hcmus.edu.vn)

Citation: Tho NA, Tien LNH, Dung TX. Land cover change and dry-season thermal patterns across the urbanizing areas in southeastern Vietnam. *Asian J Water Environ Pollut*.
doi: 10.36922/AJWEP026360256

Received: September 5, 2026

Revised: September 18, 2026

Accepted: September 20, 2026

Published online: October 22, 2026

Copyright: © 2026 Author(s). This is an Open-Access article distributed under the terms of the Creative Commons Attribution License, permitting distribution, and reproduction in any medium, provided the original work is properly cited.

Publisher's Note: AccScience Publishing remains neutral with regard to jurisdictional claims in published maps and institutional affiliations.

1. Introduction

Urban growth is a major land-system process of the 21st century.[1] Converting vegetated and agricultural land to buildings, roads, and industrial surfaces changes albedo,

roughness, soil moisture, and the partitioning of sensible and latent heat.[2] These changes contribute to the surface urban heat island phenomenon, in which satellite-observed land surface temperatures over built-up surfaces are often higher than those over surrounding vegetated land.[3] The magnitude of this thermal signal varies with climate, urban form, season, and the pace of land conversion.[4] Its consequences include higher cooling demand, outdoor heat exposure, and ecosystem stress.[1]

Impervious materials store solar energy and restrict evapotranspiration, whereas vegetation moderates surface temperature through shading and water use.[1] Evidence from Hanoi confirms that the cooling effect of urban vegetation decreases with the distance from the green space.[5] Urbanization may also affect daytime and nighttime land surface temperature differently, and satellite-derived surface temperature should not be treated as equivalent to near-surface air temperature.[6] Cross-climate reviews report substantial variation in surface urban heat island and urban cool island intensity among tropical, temperate, arid, and cold cities.[4] These findings demonstrate that context-specific and seasonally controlled observations are essential for effective urban planning.

Remote sensing provides spatially continuous observations for reconstructing urban land change over several decades.[7] The Landsat archive combines 30-m multispectral imagery with coarser thermal observations suitable for mapping land-cover conversion, vegetation condition, and surface thermal patterns.[8,9] Built-up area and the normalized difference built-up index (NDBI) are commonly associated with higher land surface temperature (LST), whereas the normalized difference vegetation index (NDVI) generally shows an inverse relationship with temperature.[10,11] Long records remain important because individual scenes can confound land-cover effects with weather, antecedent rainfall, and sensor differences.[12]

Methodological capability has expanded rapidly due to technological advancement. Cloud processing supports large-area and multi-date thermal analysis, while machine-learning and explainable models can estimate spatial temperature variation.[13-15] Local Climate Zone frameworks provide a standardized basis for comparing urban form and thermal conditions.[16] Despite these advances, transparent radiometric correction, consistent seasonal sampling, and interpretable indices remain relevant. Recent Landsat research shows that product selection and NDVI-based emissivity assumptions can materially affect surface-temperature estimates.[17,18] A reproducible index-based workflow therefore remains valuable when detailed urban morphology or dense meteorological observations are unavailable.

Technology choices determine what a comparison can legitimately explain. Although prediction models can estimate spatial temperature variation, a high predictive score does not demonstrate a causal relationship between an individual predictor and the observed warming.[14] Satellite-product selection changes the spatial and temporal representation of surface heat, making suitability a question of research scale rather than nominal pixel size alone.[18] These issues are particularly relevant at industrial fringes where roofs, bare soil, and crops coexist within a thermal footprint. For instance, Landsat studies in India and Turkey illustrate comparable applications, although their observation periods and local land-cover conditions differ from southeastern Vietnam.[7,19] A transparent comparison should therefore distinguish directly mapped variables from those derived from endpoint totals, while explicitly identifying conclusions that require supplementary spatial or temporal evidence.

Southeast Asia is an important test region because rapid urban and industrial expansion directly coincides with a humid tropical climate and high population exposure. A harmonized dataset for Manila, Bangkok, and Jakarta shows that built area, vegetation, industrial land, and socioeconomic activity jointly structure extreme-heat clusters.[20] Similarly, previous Vietnamese studies have documented thermal change in rapidly urbanizing landscapes.[5,21,22] In Hanoi, urban green space reduced summer LST by up to 2.14 °C near vegetation, and a simulated 10% vegetation gain lowered citywide summer LST by 0.56 °C.[5]

Research in Vietnam has focused mainly on Hanoi and Ho Chi Minh City, leaving fewer comparable assessments of the industrializing provinces in the Southern Key Economic Region. Tay Ninh experienced substantial land-use and land-cover change between 1988 and 2023.[21] A separate regional analysis documented LST evolution in rapidly urbanizing areas of Vietnam and Cambodia.[22] Collectively, these studies establish local relevance but do not provide a harmonized comparison of urban areas at contrasting stages of transformation.

Binh Duong, Tay Ninh, and Binh Phuoc form a compelling comparative framework for analyzing intensive corridor development, center-and-road expansion, and clustered growth around emerging industrial nodes. Although a common seasonal window and comparable processing rules support descriptive comparison, they do not isolate urbanization effects from meteorological or sensor differences. Research in western Ethiopia demonstrates that development form modifies the relationship between land conversion and surface heat.[23] Seasonal analyses in Turkey show that background climate

alters the thermal expression of urbanization, while an Indian city study demonstrates the advantage of linking land-cover trajectories to LST.[24,25]

Accordingly, this study aims to: (i) map impervious-surface expansion between 1999 and 2024; (ii) describe vegetation condition using NDVI; (iii) map dry-season surface thermal classes; and (iv) compare absolute change and normalized thermal footprints across three urban study masks. Its contribution is a regional comparison of contrasting development patterns using a common set of interpretable indicators. The analysis distinguishes mapped area from validated area, high-temperature footprints from urban–rural temperature contrasts, and observed surface temperature from near-surface air temperature.

This study is framed as a regional diagnostic rather than a universal causal model. It asks where impervious growth and high surface temperatures co-occur, how vegetation persistence differentiates the three trajectories, and which stages of development offer the greatest opportunity for intervention. The selected eight February scenes establish a sampled dry-season diagnostic baseline; they do not measure an annual trend or the maximum human heat exposure.

2. Materials and methods

2.1. Study areas and observations

We analyzed selected urban areas within the former provinces of Binh Duong, Tay Ninh, and Binh Phuoc in southeastern Vietnam (Figure 1). Their stated study extents were 99,463.933, 25,684.281, and 8,645.229 ha, respectively; these represent the study masks rather than the entire provinces. Eight February acquisitions spanning 1999–2024 were utilized: Landsat 5 Thematic Mapper (TM) from 1999, 2004, 2007, and 2010, along with Landsat 8 Operational Land Imager/Thermal Infrared Sensor (OLI/TIRS) from 2015, 2017, 2020, and 2024 (Table 1). Scene cloud cover ranged from 0% to 3%. Images were co-registered on a 30-m grid, clipped to the study masks, and visually compared with historical Google Earth imagery. Figure 2 summarizes the processing workflow.

The fixed study masks comprised selected former ward and commune units rather than whole provinces. The Tay Ninh mask included Chau Thanh, Tan Ninh, Ninh Thanh, Thanh Dien, Hoa Thanh, and Long Hoa. The Binh Duong mask included Di An, Binh Hoa, Lai Thieu, Tan Dong Hiep, An Phu, Thuan Giao, Thuan An, Thu Dau Mot, Phu Loi, Tan Khanh, Chanh Hiep, Binh Duong, Tan Hiep, Tan Uyen, Vinh Tan, Hoa Loi, Thoi Hoa, Phu An, Chanh Phu Hoa, Long Nguyen, Ben Cat, and Bau Bang. The Binh Phuoc mask covered Binh Phuoc ward in the former Dong Xoai City. These urbanizing localities were compared based on their stated, unequal study extents rather than as equal-area samples. The imagery was drawn from United States Geological Survey Landsat Collection 2 Level-1 Terrain Precision, Path 125/Row 052.

The output grid did not represent native thermal resolution: TM band 6 and TIRS band 10 were acquired at 120 and 100 m, respectively.[8,9] While sampling in February reduces seasonality, it cannot control for overpass weather conditions or atmospheric moisture.

Table 1. Documented Landsat acquisition dates used in the comparison

No.	Acquisition date	Sensor	Cloud cover (%)
1	February 13, 1999	Landsat 5 TM	3.00
2	February 11, 2004	Landsat 5 TM	3.00
3	February 3, 2007	Landsat 5 TM	0.00
4	February 11, 2010	Landsat 5 TM	1.00
5	February 9, 2015	Landsat 8 OLI/TIRS	0.09
6	February 14, 2017	Landsat 8 OLI/TIRS	0.52
7	February 7, 2020	Landsat 8 OLI/TIRS	2.03
8	February 18, 2024	Landsat 8 OLI/TIRS	0.06

Note: Cloud cover is scene-wide rather than a pixel-level quality mask. Abbreviations: OLI: Operational Land Imager; TIRS: Thermal Infrared Sensor; TM: Thematic Mapper.

2.2. Classification and validation framework

Maximum likelihood classification (MLC) was employed to distinguish impervious surfaces, pervious surfaces, and water, with the pervious land class encompassing vegetation, agriculture, forest, and bare soil. Predictors comprised reflective bands (TM 1–5 and 7; OLI 2–7), near-infrared (NIR)/green and first short-wave infrared (SWIR1)/green ratios. TM 5–4–3 and OLI 6–5–4 composites supported training interpretation. **Equation 1** assigns feature vector x to the largest discriminant score; μ_i, Σ_i, and P_i denote class mean, covariance, and prior probability, respectively. Superscripted T denotes transpose; the determinant and inverse of Σ_i describe class dispersion.

$$g_i(x) = -\frac{1}{2}\ln(|\Sigma_i|) - \frac{1}{2}(x-\mu_i)^T \Sigma_i^{-1}(x-\mu_i) + \ln(P_i) \quad (1)$$

Equations 2 and **3** specify overall accuracy (OA) and kappa. Confusion-matrix rows are reference classes, and columns are mapped classes; n_{ii} is diagonal agreement,

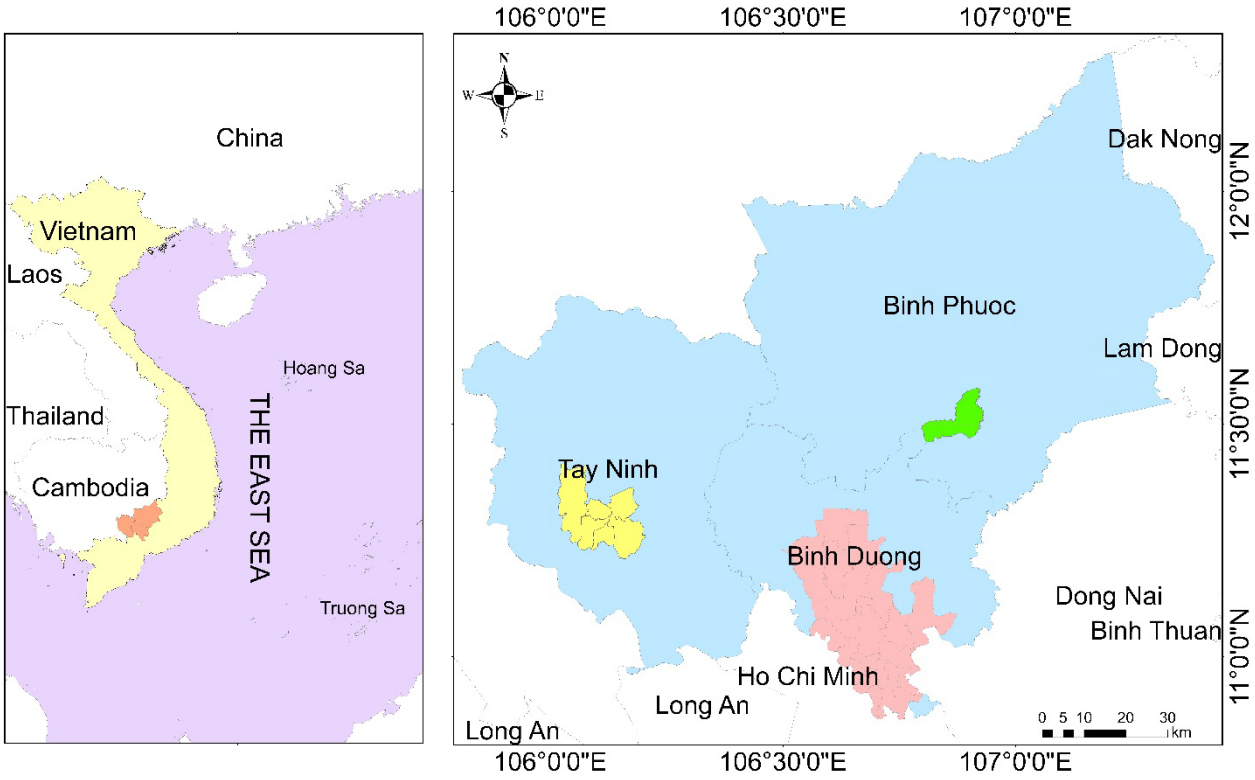


Figure 1. Location and extent of the Binh Duong, Tay Ninh, and Binh Phuoc urban study areas in southeastern Vietnam

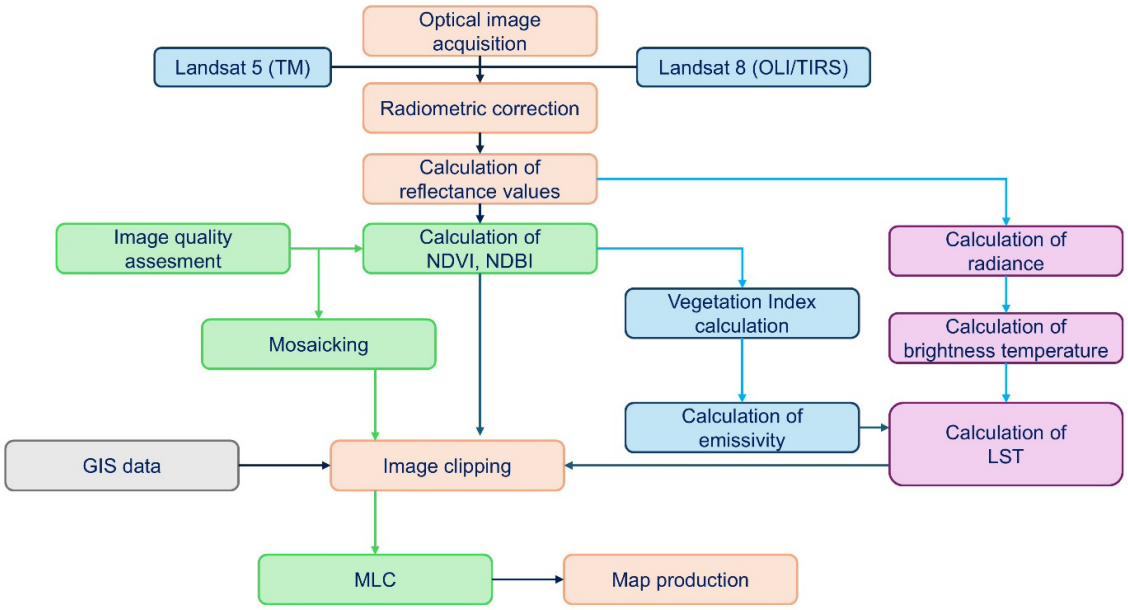


Figure 2. Landsat processing and classification workflow. Optical reflectance supplies vegetation information for emissivity; thermal radiance is calculated independently from thermal-band digital numbers.
Abbreviations: GIS: Geographic information system; LST: Land surface temperature; MLC: Maximum likelihood classification; NDBI: Normalized difference built-up index; NDVI: Normalized difference vegetation index; OLI: Operational Land Imager; TIRS: Thermal Infrared Sensor; TM: Thematic Mapper.

N is the sample total, k is the class count, p is OA, and p_e is expected agreement from row and column marginals. Because independent date-specific confusion matrices were not available, mapped areas are reported without error adjustment. Disproportionate validation sampling would require design-consistent weights.[26]

$$\mathrm{OA} = \frac{\sum_{i=1}^{k} n_{ii}}{N} \tag{2}$$

$$\kappa = \frac{p - p_e}{1 - p_e} \tag{3}$$

2.3. Optical calibration and spectral indices

Equation 4 converts digital number Q_{cal} to spectral radiance L_λ using metadata gain M_L and offset *et al.* For legacy TM calibration, **Equation 5** expresses the equivalent relation using minimum/maximum radiance and digital number endpoints.[27] Radiance units are W m^{-2} sr^{-1} μm^{-1}. These are alternative product-dependent routes rather than successive corrections.

$$L_\lambda = M_L Q_{\mathrm{cal}} + A_L \tag{4}$$

$$L_\lambda = \frac{L_{MAX} - L_{MIN}}{Q_{CAL\ MAX} - Q_{CAL\ MIN}} \left(Q_{CAL} - Q_{CAL\ MIN}\right) + L_{MIN} \tag{5}$$

Equations 6 and **7** use reflectance gain M_ρ, offset A_ρ, and solar elevation θ_{SE} to obtain top-of-atmosphere reflectance ρ_λ. **Equation 8** is the alternative legacy TM route, where d is Earth–Sun distance in astronomical units, $ESUN_\lambda$ is band-specific exoatmospheric irradiance, and θ is solar elevation. Historical *ESUN* tables must not be mixed with a different Landsat Collection calibration convention.[28] Top-of-atmosphere reflectance is not atmospherically corrected surface reflectance.

$$\rho_\lambda{}' = M_\rho Q_{\mathrm{cal}} + A_\rho \tag{6}$$

$$\rho_\lambda = \frac{\rho_\lambda{}'}{\sin\left(\theta_{\mathrm{SE}}\right)} \tag{7}$$

$$\rho_\lambda = \frac{\pi\, L_\lambda d^2}{ESUN_\lambda \sin\theta} \tag{8}$$

Normalized difference vegetation index and NDBI were computed using **Equations 9** and **10**. RED, NIR, and SWIR denote red, near-infrared, and first shortwave-infrared reflectance, respectively, which correspond to TM bands 3/4/5 and OLI bands 4/5/6. NDBI represents an ancillary indicator rather than an impervious fraction; bright dry soil may also yield positive values.

$$\mathrm{NDVI} = \frac{\rho_{\mathrm{NIR}} - \rho_{\mathrm{RED}}}{\rho_{\mathrm{NIR}} + \rho_{\mathrm{RED}}} \tag{9}$$

$$\mathrm{NDBI} = \frac{\rho_{\mathrm{SWIR}} - \rho_{\mathrm{NIR}}}{\rho_{\mathrm{SWIR}} + \rho_{\mathrm{NIR}}} \tag{10}$$

2.4. Emissivity and thermal calculation

Vegetation fraction P_v was computed using fixed NDVI endpoints 0.2 and 0.5 (**Equation 11**). Values were bounded at zero below 0.2 and one above 0.5. For soil–vegetation mixtures, **Equation 12** yields emissivity ε between 0.986 and 0.990.[29] A water value of 0.99 requires independently identified water pixels; NDVI < 0 alone is insufficient. These assumptions are not material-specific validation for roofs, asphalt, or concrete.

$$P_v = \left(\frac{\mathrm{NDVI} - \mathrm{NDVI}_{\min}}{\mathrm{NDVI}_{\max} - \mathrm{NDVI}_{\min}}\right)^2 \tag{11}$$

$$\varepsilon = 0.004 P_v + 0.986 \tag{12}$$

Equation 13 converts thermal radiance to brightness temperature T_B using metadata constants K_1 and K_2. **Equation 14** applies emissivity correction with effective wavelength λ in meters and the second radiation constant ρ = hc/kB ≈ 1.438×10^{-2} m K, where h, c, and kB are Planck's constant, the speed of light, and Boltzmann's constant. Both T_B and T_s are expressed in kelvins. **Equation 15** converts T_s into degrees Celsius.

$$T_B = \frac{K_2}{\ln\left(\frac{K_1}{L_\lambda} + 1\right)} \tag{13}$$

$$T_s = \frac{T_B}{1 + \left(\frac{\lambda \times T_B}{\rho}\right) \ln\left(\varepsilon\right)} \tag{14}$$

$$\mathrm{LST}_{^\circ\mathrm{C}} = T_s - 273.15 \tag{15}$$

This emissivity-based approximation does not explicitly solve atmospheric transmission or upwelling/downwelling radiance. It is not equivalent to the atmosphere-corrected United States Geological Survey Collection 2 surface-temperature product.[30] Absolute thermal thresholds remain conditional on retrieval assumptions.

For a controlled sensitivity example, fixing T_B at 300 K and λ at 10.9 μm yields 27.815 °C and 27.537 °C at emissivities of 0.986 and 0.990, respectively. The 0.278 °C difference reflects a parameter sensitivity rather than an observed site error or confidence interval. Its effect on mapped hotspot area cannot be determined without the near-threshold temperature distribution.

2.5. Descriptive comparison

Mapped hectares were calculated by multiplying the projected 30-m pixel counts by 0.09. Net gain was

defined as the 2024 area minus the 1999 area, which was subsequently divided by 25 to yield the endpoint-average annual gain. The expansion multiple was calculated by dividing final area by initial area, from which the twenty-fifth root minus one yields the compound annual growth fraction. Area shares were normalized using the stated study-mask extents. The >36 °C class was nested within >34 °C. Ratios between hot and impervious totals were interpreted as aggregate comparisons rather than spatial intersections; furthermore, NDVI-threshold areas may overlap with MLC classes. No inferential test, pixel-level regression, urban–rural temperature contrast, or human-exposure metric was estimated. Two decimal places in the area tables retained the arithmetic of 0.09-ha grid cells; they did not represent classification accuracy. Narrative areas were rounded to the nearest hectare, whereas rates and shares were calculated from the unrounded mapped totals.

3. Results

3.1. Impervious expansion

Impervious land increased in all three areas between 1999 and 2024. In Binh Duong, its extent increased from 1,981 to 31,862 ha, representing a net increase of 29,882 ha (Table 2). The 16.09-fold increase corresponded to an endpoint compound rate of 11.8% per year. Mapped expansion was strongest in the south and extended toward the central area, where separate built-up patches increasingly coalesced (Figure 3). This represents a spatial interpretation of the selected maps rather than a measured rate of corridor connectivity.

Impervious land in Tay Ninh expanded from 373 to 6,783 ha, with a gain of 6,411 ha and an 18.20-fold expansion. Its 12.3% annual compound rate exceeded Binh Duong's, although its absolute gain was much smaller. Growth remained concentrated around administrative centers and transport axes (Figure 4). Impervious land in Binh Phuoc increased from 291 to 3,333 ha, with an addition of 3,042 ha, equivalent to an 11.44-fold increase and a 10.2% annual compound rate. Its maps showed clustered development around Dong Xoai and industrial nodes (Figure 5).

Table 2 separates absolute growth from growth relative to the starting footprint. Binh Duong recorded a net gain almost five times that of Tay Ninh and nearly 10 times that of Binh Phuoc. Tay Ninh's larger multiplier partly reflects its small initial area. Therefore, "fastest urbanization" lacks a unique meaning without specifying the metric. The endpoint-average gains were 1,195, 256, and 122 ha per year for Binh Duong, Tay Ninh, and Binh Phuoc, respectively; however, these endpoint totals do not indicate the precise timing of growth acceleration within the 25-year interval.

3.2. Vegetation condition

In 2024, land with NDVI > 0.4 occupied 48,585 ha in Binh Duong, 18,802 ha in Tay Ninh, and 6,593 ha in Binh Phuoc (Table 3). These correspond to 48.8%, 73.2%, and 76.3% of the stated masks. Binh Duong therefore retained the largest absolute threshold area but the smallest proportional coverage. The maps suggest more continuous non-impervious surroundings in Tay Ninh and outside Binh Phuoc's development clusters, compared with the coalescing Binh Duong corridor.

These threshold statistics must not be interpreted as mutually exclusive land-cover area totals. In particular, mixed pixels may satisfy NDVI > 0.4 while being assigned to another MLC class; furthermore, the pervious land class includes bare soil. Therefore, the high NDVI share in Binh Phuoc does not contradict its high mapped impervious share through simple addition. A common-mask cross-tabulation is required to measure overlap. Without a complete NDVI area series or landscape metrics, neither the magnitude of vegetation loss nor the degree of fragmentation is quantified.

Table 2. Impervious expansion between 1999 and 2024

Urban area	1999 area (ha)	2024 area (ha)	Net gain (ha)	Expansion multiple	CAGR (% yr^{-1})
Binh Duong	1,980.81	31,862.43	29,881.62	16.09	11.8
Tay Ninh	372.69	6,783.39	6,410.70	18.20	12.3
Binh Phuoc	291.24	3,333.24	3,042.00	11.44	10.2

Notes: Rates are calculated from endpoints and do not imply constant annual growth. Areas are mapped estimates. Displayed areas retain exact 0.09-ha pixel-count increments, which do not imply validated measurement precision; values reported in the main text are rounded to the nearest whole hectare.
Abbreviation: CAGR: Compound annual growth rate.

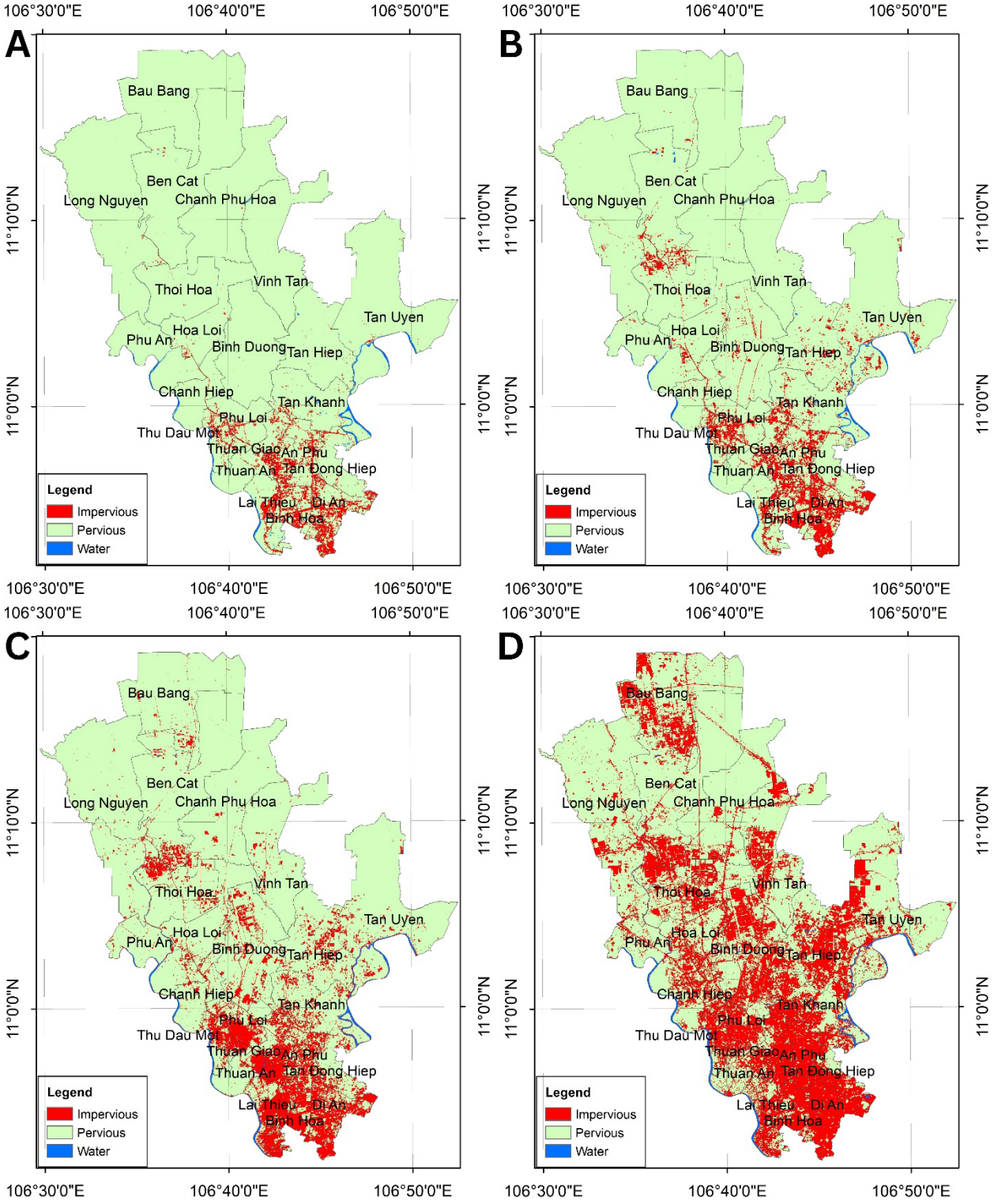


Figure 3. Mapped impervious surfaces in the Binh Duong urban area. Panels show data from (A) 2004, (B) 2007, (C) 2015, and (D) 2024. Impervious, pervious, and water are the three MLC classes, with the pervious land class including bare soil as well as vegetation.
Abbreviation: MLC: Maximum likelihood classification.

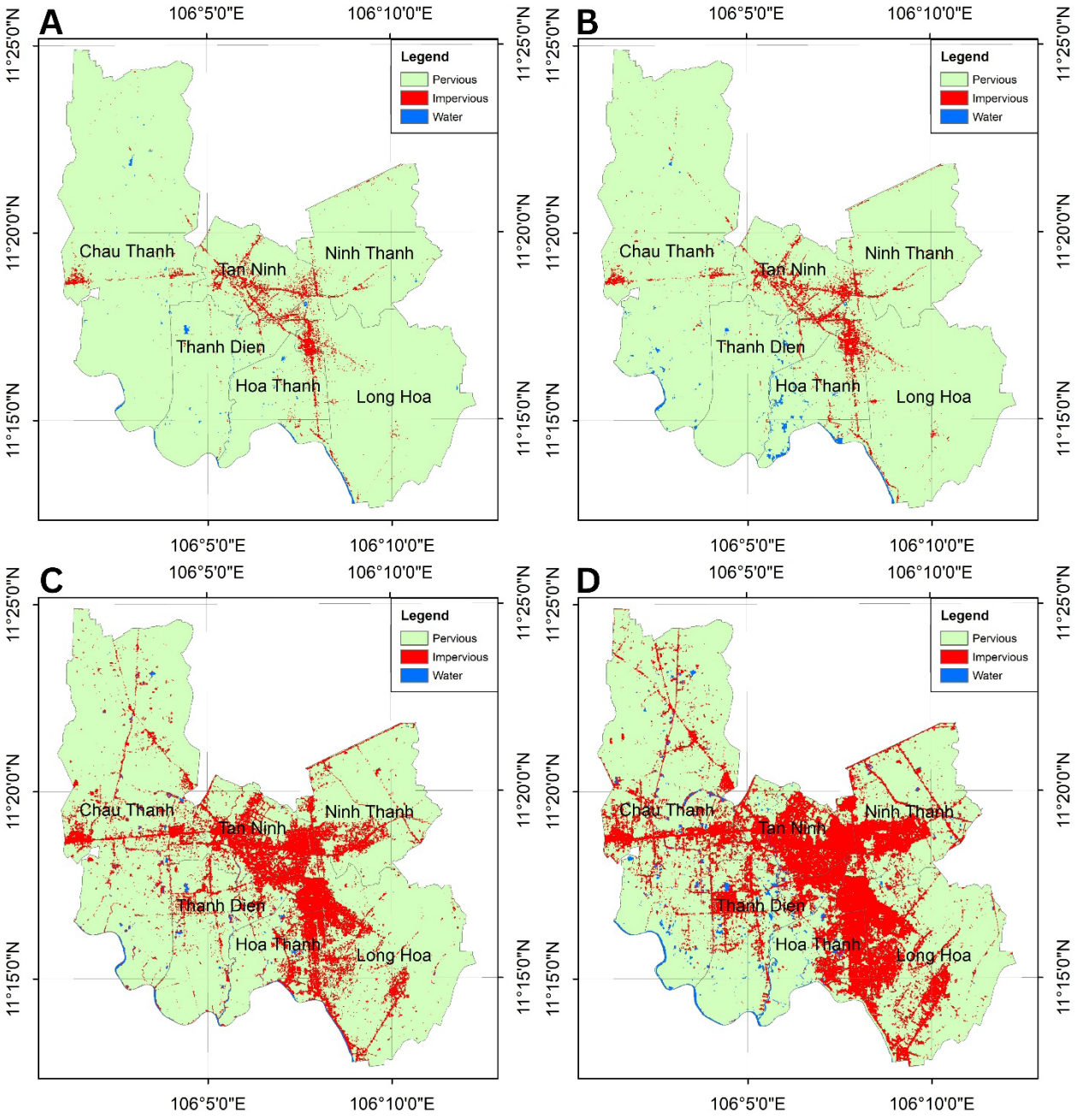


Figure 4. Mapped impervious surfaces in the Tay Ninh urban area. Panels show data from (A) 2004, (B) 2007, (C) 2015, and (D) 2024. Impervious, pervious, and water are the three MLC classes, with the pervious land class including bare soil as well as vegetation.
Abbreviation: MLC: Maximum likelihood classification.

3.3. Surface thermal footprints

In 2024, 8,857 ha in Binh Duong had an estimated LST above 34 °C, including 1,004 ha above 36 °C (Figure 6; Table 4). The hotter class represented 11.3% of the > 34 °C footprint and was not present in the 2004 classification. Hot patches appeared concentrated along the southern and central industrial corridor. The aggregate hot-area-to-impervious-area ratio was 27.8%; however, this does not mean that 27.8% of impervious pixels exceeded 34 °C, since the two mapped layers were not intersected.

In Tay Ninh, 81 ha had an estimated LST above 34 °C and 15 ha above 36 °C, principally around Tan Ninh, Hoa

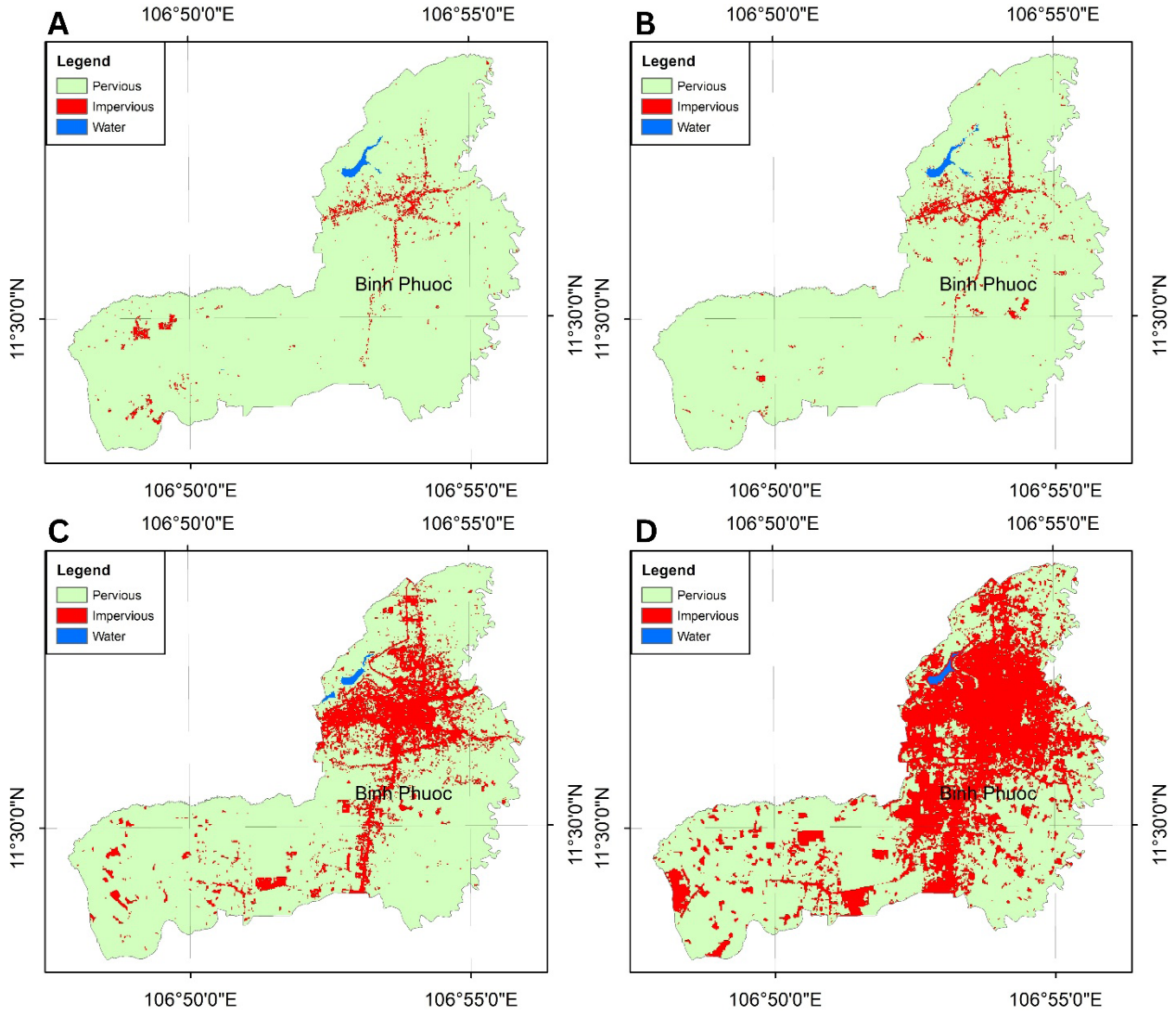


Figure 5. Mapped impervious surfaces in the Binh Phuoc urban area. Panels show data from (A) 2004, (B) 2007, (C) 2015, and (D) 2024. Impervious, pervious, and water are the three MLC classes, with the pervious land class including bare soil as well as vegetation.
Abbreviation: MLC: Maximum likelihood classification.

Table 3. Land exceeding the NDVI threshold in 2024

Urban area	Stated extent (ha)	NDVI > 0.4 (ha)	Share (%)
Binh Duong	99,463.933	48,585.06	48.8
Tay Ninh	25,684.281	18,801.90	73.2
Binh Phuoc	8,645.229	6,593.22	76.3

Notes: Threshold areas may overlap with mixed pixels assigned to other land-cover classes; hence, shares are conditional on the stated study-mask extents. Values reported in the main text are rounded to the nearest whole hectare.
Abbreviation: NDVI: Normalized difference vegetation index.

Thanh, and development axes (Figure 7). In Binh Phuoc, the areas exceeding 34 °C and 36 °C were 348 and 62 ha, respectively (Figure 8). Table 4 summarizes these footprints. No area below 26 °C was reported in Binh Phuoc's 2024 classification. This is a scene-specific absence rather than proof of disappearing cool conditions throughout the year.

The proportion of the area exceeding 34 °C that also exceeded 36°C was 18.2% in Tay Ninh and 17.8% in Binh Phuoc, which were higher than Binh Duong's 11.3%. Yet Tay Ninh's entire hot footprint was only 81 ha. Therefore, a within-hotspot fraction yields a different ordering from the total hot area and must not be used in isolation to rank overall thermal conditions. Small footprints may also be particularly sensitive to classification errors and temperatures near the chosen threshold.

3.4. Comparison using stated study extents

Normalization using stated study extents clarifies the influence of unequal study areas (Table 5). Impervious shares increased from 1.99% to 32.03% in Binh Duong, from 1.45% to 26.41% in Tay Ninh, and from 3.37% to 38.56% in Binh Phuoc. In 2024, areas with LST > 34 °C accounted for 8.91%, 0.32%, and 4.03% of the study masks in Binh Duong, Tay Ninh, and Binh Phuoc, respectively. The corresponding proportions for LST > 36 °C were 1.01%, 0.06%, and 0.72%. Binh Phuoc had the highest impervious proportion, whereas Binh Duong had the highest hot-area proportion. Therefore, impervious fraction alone does not reproduce the observed thermal ordering. Instead, materials, vegetation, observation conditions, and retrieval uncertainty remain potential contributing factors. All normalized comparisons utilized the stated study-mask extents.

The contrast between Binh Phuoc and Tay Ninh is particularly informative. Binh Phuoc comprised less than half of Tay Ninh's built-up area in 2024, yet its > 34 °C footprint was more than four times larger. Additionally, both retained high NDVI-threshold shares. These aggregate differences show that neither total impervious hectares nor a single vegetation-area percentage can account for thermal variation across the masks. The comparison identifies a question for matched spatial analysis: whether hot surfaces differ in their material composition, vegetation surroundings, or observation conditions. The present endpoint summaries are not sufficient to distinguish these explanations or estimate their separate contributions.

4. Discussion

The co-occurrence of impervious growth and warmer

Table 4. Nested high-temperature footprints in 2024

Urban area	LST > 34 °C (ha)	LST > 36 °C (ha)	>36 °Cshare of > 34 °C area (%)	>34 °C area relative to built-up area (%)
Binh Duong	8,857.44	1,004.04	11.3	27.8
Tay Ninh	81.09	14.76	18.2	1.2
Binh Phuoc	348.03	62.10	17.8	10.4

Notes: The > 36 °C class is included in the >34 °C class. The final column compares aggregate areas; it does not reflect the fraction of impervious pixels above 34 °C. Values reported in the main text are rounded to the nearest whole hectare.
Abbreviation: LST: Land surface temperature.

Table 5. Indicators normalized by the stated study extents

Indicator	Binh Duong	Tay Ninh	Binh Phuoc
1999 impervious share (%)	1.99	1.45	3.37
2024 impervious share (%)	32.03	26.41	38.56
2024 > 34 °C mask share (%)	8.91	0.32	4.03
2024 > 36 °C mask share (%)	1.01	0.06	0.72
Endpoint-average net gain (ha/year)	1,195.26	256.43	121.68

Notes: Shares are calculated relative to the stated study-mask extents. Endpoint-average gain is defined as the net mapped change divided by the 25-year interval.

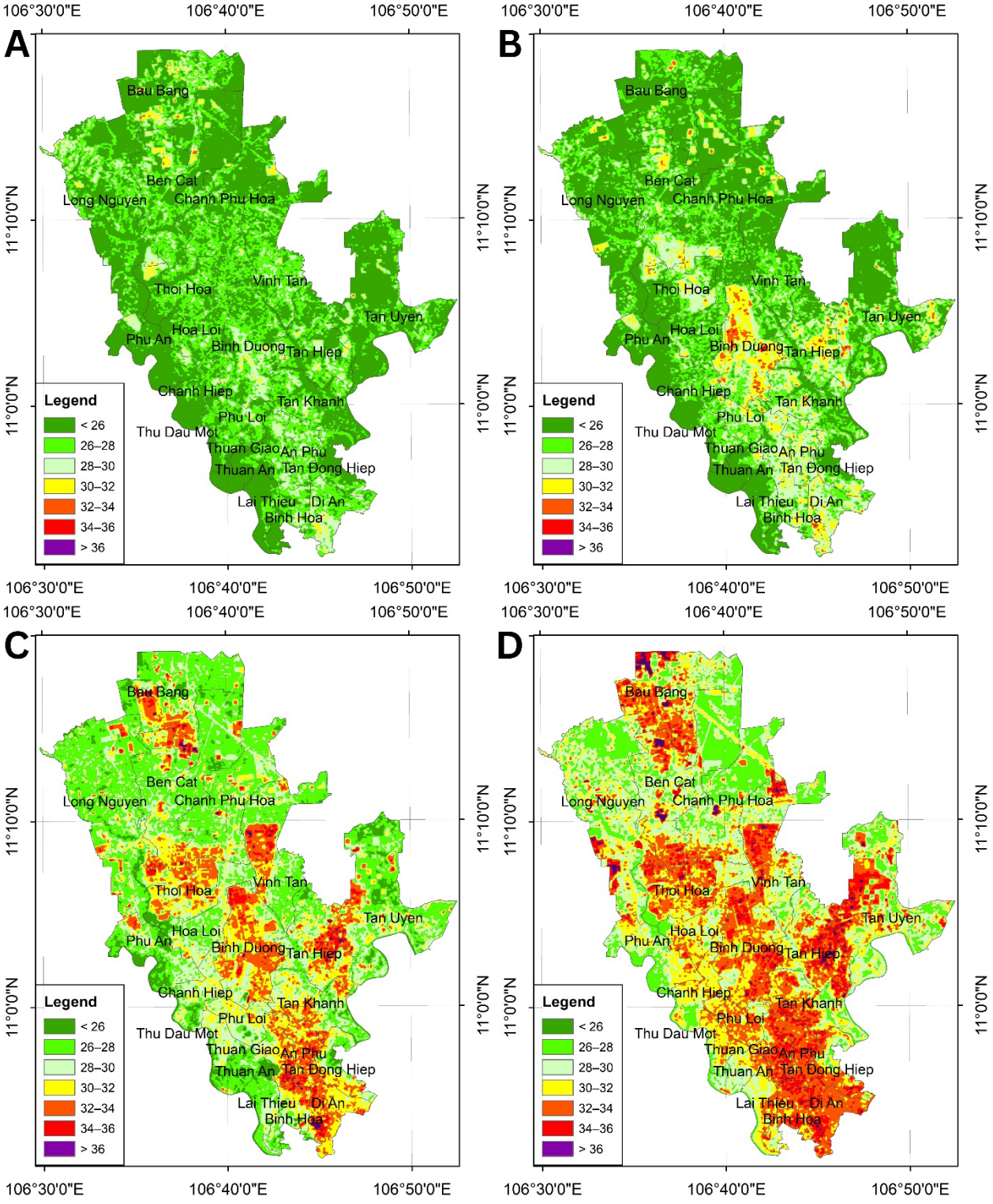


Figure 6. Mapped LST in the Binh Duong urban area. Panels show data from (A) 2004, (B) 2007, (C) 2015, and (D) 2024. Temperatures are in degrees Celsius and represent sampled February conditions under the emissivity-based retrieval assumptions.
Abbreviation: LST: Land surface temperature.

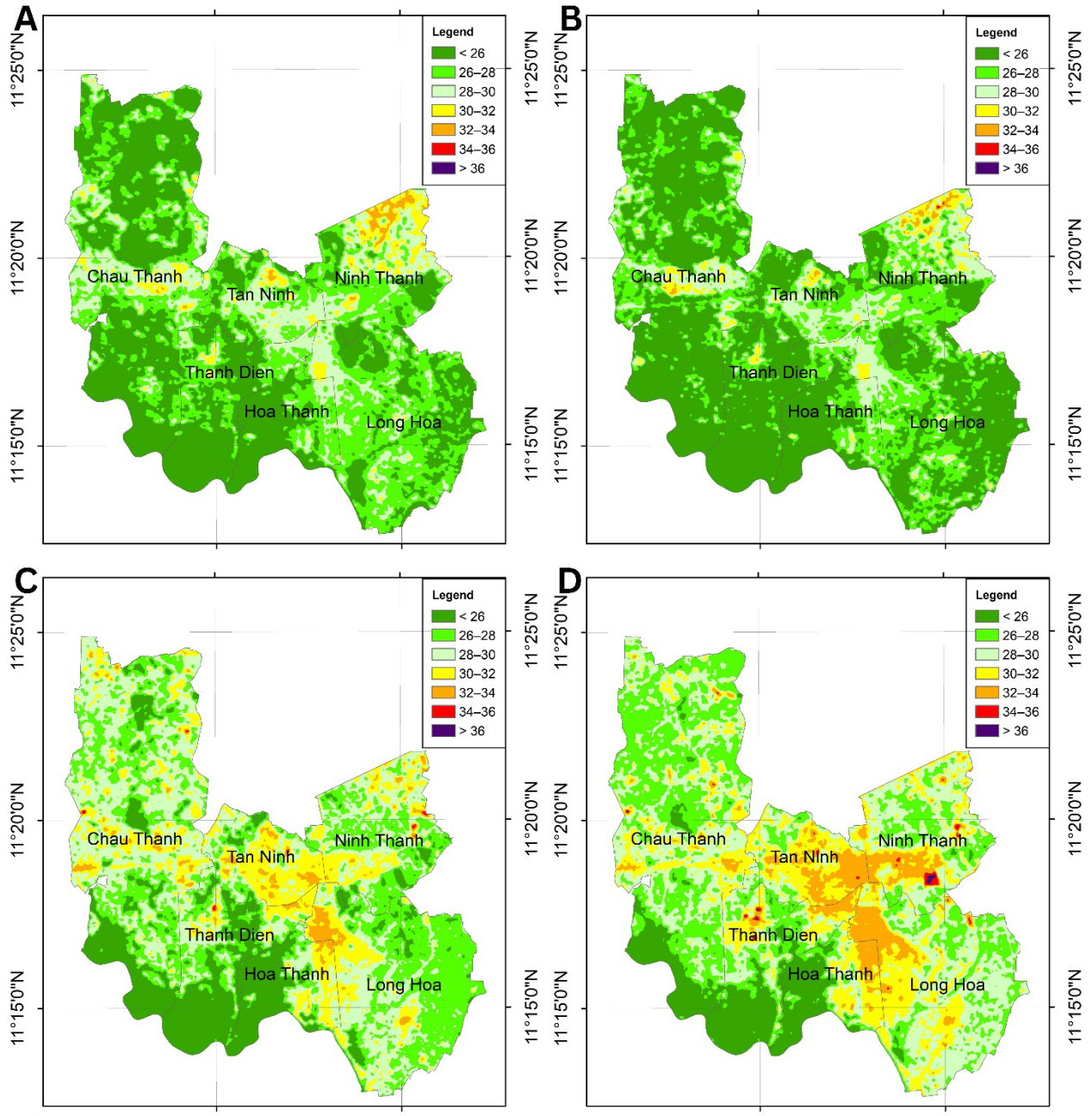


Figure 7. Mapped LST in the Tay Ninh urban area. Panels show data from (A) 2004, (B) 2007, (C) 2015, and (D) 2024. Temperatures are in degrees Celsius and represent sampled February conditions under the emissivity-based retrieval assumptions.
Abbreviation: LST: Land surface temperature.

mapped surfaces is consistent with established urban surface-energy mechanisms.[1,3] However, a common regional climate does not control scene-specific weather conditions or land-cover composition. The principal contribution of this study is the comparative analysis of absolute conversion, concentration within differently sized study-mask extents, and threshold-based thermal footprints. Crucially, the pathway labels describe map patterns rather than statistically tested development mechanisms.

Veettil *et al.* [22] documented built-up expansion from 387 to 464.3 km^2 in southern Binh Duong and an increase in maximum LST of approximately 0.024 °C per year.

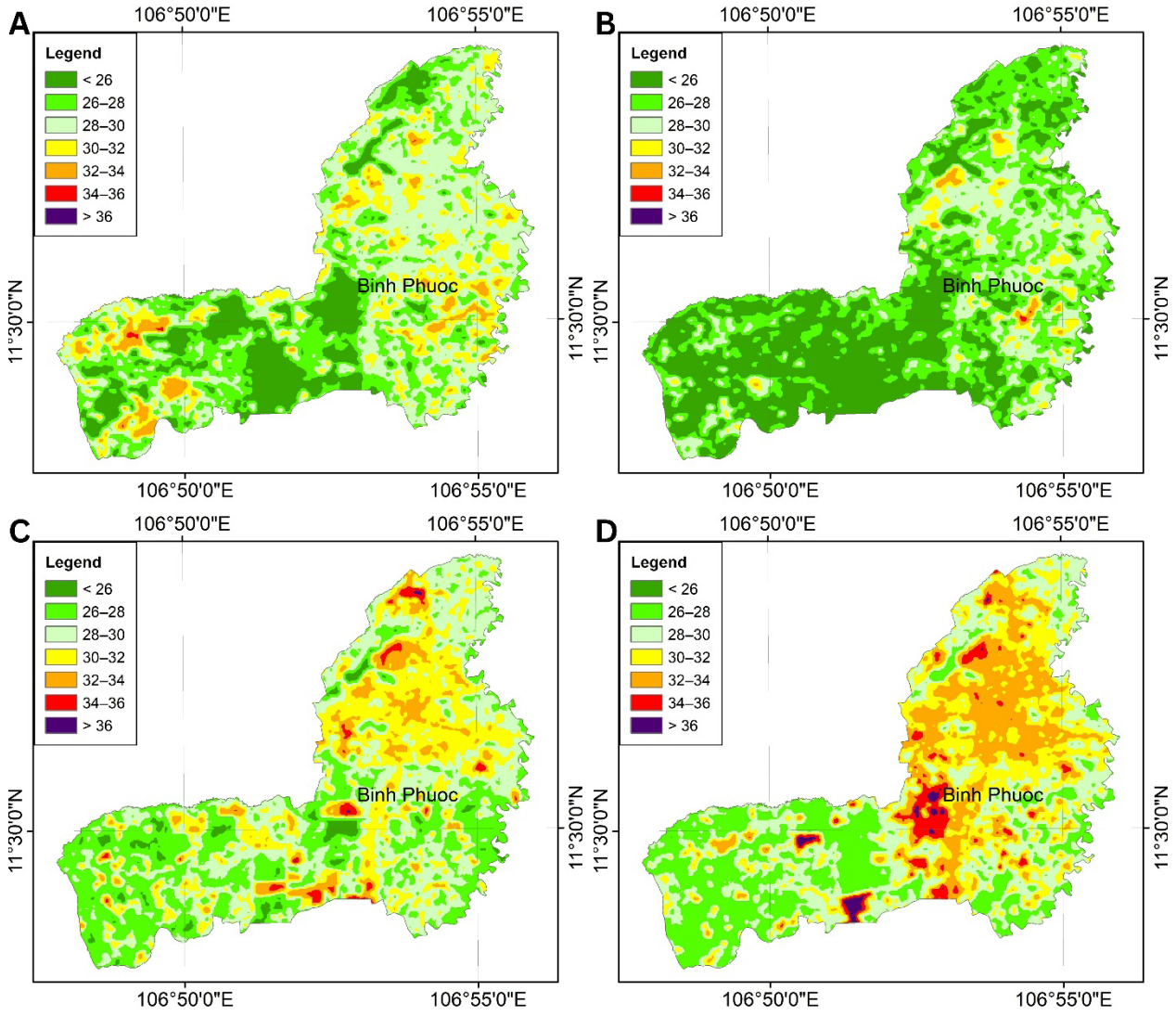


Figure 8. Mapped LST in the Binh Phuoc urban area. Panels show data from (A) 2004, (B) 2007, (C) 2015, and (D) 2024. Temperatures are in degrees Celsius and represent sampled February conditions under the emissivity-based retrieval assumptions.
Abbreviation: LST: Land surface temperature.

The present maps are consistent with the geographic concentration of that transformation, but the footprints and observation periods differ. Consequently, the temperature trend cannot be equated with the endpoint area ratios in this study. Studies in Hyderabad and New Town Kolkata provide further evidence of associations between impervious development, vegetation, and LST.[31,32]

The Tay Ninh pattern complements the province-wide analysis by Thien *et al.*,[21] which documented land use/land cover change and thermal effects from 1988 to 2023. The present urban-area mask isolates administrative and transport-led growth while showing that extreme surfaces remain spatially restricted despite an 18-fold increase in built-up area. Correspondingly, research conducted in Aligarh links built-up expansion to higher LST, while a study in Bengaluru illustrates how retained vegetation differentiates neighborhood temperatures.[25,33] These results suggest an opportunity for preventive planning before separate corridors merge.

The Binh Phuoc result illustrates why a small absolute urban footprint does not necessarily imply low local development intensity, as its mapped impervious share constitutes 38.56% of the stated study-mask extent. The absence of the coolest thermal class in the 2024 scene does not constitute evidence of annual climate change. Studies in Cuttack and Multan associate urban conversion with

thermal change,[34,35] and a decadal analysis in Madurai reports a similar directional association.[36] However, their effect sizes cannot be transferred directly to the context of Binh Phuoc. Consequently, the local cooling benefit of vegetation around emerging industrial clusters remains to be quantified.

Vegetation results have direct design implications. Research in Bhopal associates higher NDVI with cooler surfaces and higher NDBI with warmer surfaces.[10] Studies in Izmir and southern Iraq show that seasonality and background moisture modify these relationships.[11,24] A study in Hanoi provides locally relevant evidence: Nguyen *et al*.[5] estimated a 2.14 °C summer cooling effect near urban green spaces that declines with distance, and projected additional cooling under vegetation gain. In the context of Binh Duong, these findings support evaluating retained patches and green corridors, while establishing their cooling distance and effectiveness locally.

The water class includes rivers, lakes, ponds, and reservoirs; however, the available summaries do not provide water area by date or temperatures by distance to water. Consequently, these maps cannot quantify the cooling effect of the Saigon River, Dau Tieng Reservoir, or smaller water bodies. Impervious expansion may reduce water infiltration and increase stormwater runoff, whereas runoff warmed on exposed built surfaces could transfer heat to receiving waters. These mechanisms represent plausible pathways rather than measured impacts on stream temperature, groundwater recharge, or water quality in this study. Validating these pathways requires dated water-class area mapping, riparian buffer evaluations, land-cover-by-LST cross-tabulation, and independent hydrological and water-quality observations.

The comparison also reinforces the need to distinguish LST from air temperature. Satellite LST captures the radiometric skin temperature of surfaces at overpass time rather than human-experienced air temperature. Heatwave conditions can modify relationships between surface and air temperature.[6] Accordingly, the mapped high-temperature areas serve as screening indicators for further thermal assessment; exposure studies should also incorporate station observations, humidity, shade, and population vulnerability.

Cloud processing can extend the analysis to denser temporal archives.[13] Explainable artificial intelligence models may subsequently evaluate spatial predictors while providing more transparent contributions.[15] Although machine-learning applications in Afghanistan have demonstrated this potential, model development should follow independent validation of the underlying classification archive.[37]

Studies in Ethiopia and Mexico have demonstrated the geographic breadth of urbanization-related surface change.[23,38] Topographic controls are evident in the lower Himalayan region, whereas vegetation and water limitations shape the response in semi-arid settings.[39,40] These comparisons provide context rather than validation of the local temperature thresholds used in this study. The primary limitations of this study concern its temporal resolution and validation; specifically, the eight February observations characterize selected dry-season conditions rather than annual climatic trends. Without date-specific classification accuracy and an independent thermal benchmark, area estimates have no quantified uncertainty bounds. Resampling thermal observations to a 30-m grid does not create independent 30-m temperature measurements. The unequal study-mask extents and three aggregate study areas do not support causal regression, and the analysis does not estimate an urban–rural contrast or fragmentation metric. The scene-wide cloud percentages in Table 1 do not establish cloud and shadow fractions within each study-mask extent. Furthermore, the interpolation method applied to the native thermal pixels and the source/version of the administrative-boundary layer remain undocumented within the available processing record.

An additional limitation is the mathematical coupling between NDVI and the retrieved temperature: NDVI determines vegetation fraction and consequently emissivity through **Equations 11–14**. Therefore, any subsequent NDVI–LST regression would partly relate an input to a quantity derived from that input. An alternative emissivity source or independent thermal benchmark, along with spatially blocked analysis, is needed to distinguish ecological association from retrieval-induced dependence. Similarly, adding band ratios to MLC does not demonstrate improved accuracy without an independent comparison with the original feature set.

Urban planning priorities should reflect the observed spatial patterns. For instance, Binh Duong warrants evaluation of green-patch reconnection, shaded industrial streets, and roof or pavement performance. Tay Ninh should protect green wedges and riparian corridors before road-led development coalesces, whereas Binh Phuoc should assess vegetation buffers around emerging industrial clusters. These measures require local validation because cooling performance depends on climate, configuration, and season.[5,24]

Future attribution studies require independent classification validation, consistent valid-pixel masks, a documented atmospheric and emissivity scheme, and land-cover-by-temperature cross-tabulation. Spatially blocked machine learning models and Local Climate Zone

contrasts could subsequently be deployed to evaluate the competing explanations in this study.[14,16]

5. Conclusion

This study used a consistent Landsat and geographic information system framework to compare land-cover transformation and sampled dry-season surface thermal patterns in three urbanizing areas of southeastern Vietnam from 1999 to 2024. Impervious land expanded most in absolute terms in Binh Duong, from 1,981 to 31,862 ha. Tay Ninh recorded the largest expansion multiple, whereas Binh Phuoc exhibited the highest 2024 impervious share of its study mask. These metrics show that absolute extent, relative growth, and spatial concentration must be interpreted separately.

In 2024, areas above 34 °C covered 8,857 ha in Binh Duong, 81 ha in Tay Ninh, and 348 ha in Binh Phuoc, representing 8.91%, 0.32%, and 4.03% of the stated study masks, respectively. Land with NDVI > 0.4 remained extensive but recorded its lowest proportional coverage in Binh Duong. Rankings based on impervious share, vegetation-threshold area, and high-temperature footprint differed, showing that no single aggregate indicator sufficiently describes local thermal conditions. Without cross-tabulated rasters, the fraction of built-up land with high LST cannot be accurately estimated.

The findings support evaluating green-patch reconnection and heat-sensitive retrofits in established Binh Duong corridors, protecting green and riparian areas ahead of coalescing growth in Tay Ninh, and assessing vegetation buffers around emerging Binh Phuoc clusters. These priorities serve screening directions rather than estimates of cooling performance. The eight February observations in this study do not establish annual trends, and the lack of independent classification and thermal validation limits uncertainty assessment. Future work should use consistent valid-pixel masks, validate historical classifications, benchmark temperature retrieval methods, and intersect land-cover data with thermal classes. Nevertheless, the framework in this study supports transparent comparison and identifies locations for detailed thermal investigation. Investigating water-body cooling along with its effects on runoff, recharge, and receiving-water temperature remains a priority for spatially matched and field-supported follow-up analyses.

Acknowledgments

None.

Funding

This research is funded by University of Science, VNU-HCM under grant number T2024 - 101.

Conflict of interest

The authors declare that they have no known competing financial interests or personal relationships that could have influenced the work reported in this paper.

Author contributions

Conceptualization: Nguyen Anh Tho, Tran Xuan Dung
Formal analysis: Nguyen Anh Tho, Tran Xuan Dung
Investigation: Nguyen Anh Tho
Methodology: All authors
Writing–original draft: Nguyen Anh Tho, Tran Xuan Dung
Writing–review & editing: All authors

Availability of data

Landsat source imagery is publicly available through the United States Geological Survey.

Further disclosure

AI assistance was used for manuscript restructuring, language editing, reference formatting, and arithmetic consistency checks. No satellite observations or validation measurements were generated through this assistance.

References

1. Mohamed A, Lorestani N, Shabani F. Impact of urbanization on land surface temperature: a global perspective. *Curr Res Environ Sustain*. 2025;10:100315.

   doi: 10.1016/j.crsust.2025.100315

2. Sinha S, Banerjee A. A systematic review of land use and land cover changes and their influence on urban heat island dynamics. *Discov Geosci*. 2025;3(1):253.

   doi: 10.1007/s44288-025-00359-4

3. Halefom A, He Y, Nemoto T, *et al*. The impact of urbanization-induced land use change on land surface temperature. *Remote Sens (Basel)*. 2024;16(23):4502.

   doi: 10.3390/rs16234502

4. Khan MS, Ullah S, Chen L. Variations in surface urban heat island and urban cool island intensity: a review across major climate zones. *Chin Geogr Sci*. 2023;33(6):983-1000.

   doi: 10.1007/s11769-023-1375-8

5. Nguyen KA, Thai MT, Melkamu T, Le TV, Liou YA. Quantifying the cooling intensity of urban green spaces (UGSs) on land surface temperature (LST) in Hanoi metropolitan area, Vietnam. *City Environ Interact*. 2025;28:100264.

   doi: 10.1016/j.cacint.2025.100264

6. Wang N, Chen J, He T, *et al*. Understanding the differences

in the effect of urbanization on land surface temperature and air temperature in China: insights from heatwave and non-heatwave conditions. *Environ Res Lett*. 2023;18(10):104038.

doi: 10.1088/1748-9326/acfc58

7. Mishra VK, Verma KK, Pant T, Upadhyay GM, Singh PS, Soni PK. Analysis of urbanization impact on land surface temperature variability by using Landsat imagery. *SN Comput Sci*. 2024;5(7):863.

doi: 10.1007/s42979-024-03226-0

8. United States Geological Survey. Landsat 5. Landsat Missions. Accessed September 4, 2026. https://www.usgs.gov/landsat-missions/landsat-5

9. United States Geological Survey. Landsat 8. Landsat Missions. Accessed September 4, 2026. https://www.usgs.gov/landsat-missions/landsat-8

10. Singh P, Verma P, Chaudhuri AS, Singh VK, Rai PK. Evaluating the relationship between urban heat island and temporal change in land use, NDVI and NDBI: a case study of Bhopal city, India. *Int J Environ Sci Technol*. 2024;21(3):3061-3072.

doi: 10.1007/s13762-023-05141-y

11. Kadhum SA, Awad A, Abed SA, Janaydeh M, Al-Khayat A, Al-Hemoud A. Land surface temperature and NDVI patterns in the petroleum and non-petroleum regions in Southern Iraq (Al-Basra). *Environ Dev Sustain*. 2024;28(2):4427-4451.

doi: 10.1007/s10668-024-05145-9

12. Adeyeri OE, Folorunsho AH, Ayegbusi KI, *et al*. Land surface dynamics and meteorological forcings modulate land surface temperature characteristics. *Sustain Cities Soc*. 2024;101:105072.

doi: 10.1016/j.scs.2023.105072

13. Moyo B, Schröder D, Moreri K. Cloud-computing trend analysis of urbanization impacts on land surface temperature and electricity demand in Gaborone, Botswana. *Remote Sens Earth Syst Sci*. 2025;8(1):283-306.

doi: 10.1007/s41976-024-00171-7

14. Tanoori G, Soltani A, Modiri A. Machine learning for urban heat island (UHI) analysis: predicting land surface temperature (LST) in urban environments. *Urban Clim*. 2024;55:101962.

doi: 10.1016/j.uclim.2024.101962

15. Mallick J, Alqadhi S. Explainable artificial intelligence models for proposing mitigation strategies to combat urbanization impact on land surface temperature dynamics in Saudi Arabia. *Urban Clim*. 2025;59:102259.

doi: 10.1016/j.uclim.2024.102259

16. Rahmani N, Sharifi A. Urban heat dynamics in Local Climate Zones (LCZs): a systematic review. *Build Environ*. 2025;267:112225.

doi: 10.1016/j.buildenv.2024.112225

17. Bobáľová H, Opravil Š. Improving Landsat land surface temperature estimation in Google Earth Engine using NDVI-based emissivity. *Adv Space Res*. 2026;77(3):3281-3299.

doi: 10.1016/j.asr.2025.11.085

18. Hurduc A, Ermida SL, DaCamara CC. On the suitability of different satellite land surface temperature products to study surface urban heat islands. *Remote Sens (Basel)*. 2024;16(20):3765.

doi: 10.3390/rs16203765

19. Altıner F, Bingöl F. Spatio-temporal assessment of land surface temperature, vegetation cover, and built-up areas using LST, NDVI, and NDBI in Balıkesir, Türkiye (1985-2025). *Sustainability*. 2025;17(20):9245.

doi: 10.3390/su17209245

20. Pagkalinawan H, Delina LL, Macagba SFA. Gridded dataset on land surface temperature and selected environmental and socioeconomic features in Southeast Asian metropolises. *Data Brief*. 2024;57:110848.

doi: 10.1016/j.dib.2024.110848

21. Thien BB, Phuong VT, Huong DTV. Investigating land cover changes and their impact on land surface temperature in Tay Ninh province, Vietnam. *Environ Monit Assess*. 2024;197(1):75.

doi: 10.1007/s10661-024-13519-9

22. Veettil BK, Costi J, Teck V, Puri V. Land surface temperature evolution in rapidly urbanizing areas of Southeast Asia: studies from Vietnam and Cambodia. *PLoS One*. 2025;20(10):e0328750.

doi: 10.1371/journal.pone.0328750

23. Dibaba WT. Urbanization-induced land use/land cover change and its impact on surface temperature and heat fluxes over two major cities in Western Ethiopia. *Environ Monit Assess*. 2023;195(9):1083.

doi: 10.1007/s10661-023-11698-5

24. Isinkaralar O, Isinkaralar K, Yilmaz D, Öztürk S. Multi-dimensional analysis of land use/land cover and urbanization on seasonal variation of land surface temperature in İzmir, Türkiye. *Landsc Ecol Eng*. 2025;21(1):133-150.

doi: 10.1007/s11355-024-00628-3

25. Khan D, Bano S, Khan N. Spatio-temporal analysis of urbanization effects: unravelling land use and land cover dynamics and their influence on land surface temperature in Aligarh City. *Geol Ecol Landsc*. 2025;9(4):1326-1350.

doi: 10.1080/24749508.2024.2409488

26. Olofsson P, Foody GM, Herold M, Stehman SV, Woodcock CE, Wulder MA. Good practices for estimating area and

assessing accuracy of land change. *Remote Sens Environ*. 2014;148:42-57.

doi: 10.1016/j.rse.2014.02.015

27. Chander G, Markham BL, Helder DL. Summary of current radiometric calibration coefficients for Landsat MSS, TM, ETM+, and EO-1 ALI sensors. *Remote Sens Environ*. 2009;113(5):893-903.

doi: 10.1016/j.rse.2009.01.007

28. United States Geological Survey. Using the USGS Landsat Level-1 Data Product. Landsat Missions. Accessed September 4, 2026. https://www.usgs.gov/landsat-missions/using-usgs-landsat-level-1-data-product

29. Sobrino JA, Jiménez-Muñoz JC, Paolini L. Land surface temperature retrieval from LANDSAT TM 5. *Remote Sens Environ*. 2004;90(4):434-440.

doi: 10.1016/j.rse.2004.02.003

30. United States Geological Survey. Landsat Collection 2 Surface Temperature. Landsat Missions. Accessed September 4, 2026. https://www.usgs.gov/landsat-missions/landsat-collection-2-surface-temperature

31. Suthar G, Singh S, Kaul N, Khandelwal S. Understanding the multifaceted influence of urbanization, spectral indices, and air pollutants on land surface temperature variability in Hyderabad, India. *J Clean Prod*. 2024;470:143284.

doi: 10.1016/j.jclepro.2024.143284

32. Mahata B, Sankar Sahu S, Sardar A, Laxmikanta R, Maity M. Spatiotemporal dynamics of land use/land cover (LULC) changes and its impact on land surface temperature: a case study in New Town Kolkata, eastern India. *Reg Sustain*. 2024;5(2):100138.

doi: 10.1016/j.regsus.2024.100138

33. Keerthi Naidu BN, Chundeli FA. Assessing LULC changes and LST through NDVI and NDBI spatial indicators: a case of Bengaluru, India. *GeoJournal*. 2023;88(4):4335-4350.

doi: 10.1007/s10708-023-10862-1

34. Patra PK, Behera D, Chettry V, Jena KM, Goswami S, Jothimani M. Geospatial analysis of unplanned urbanization: impact on land surface temperature and habitat suitability in Cuttack, India. *Discov Sustain*. 2025;6(1):118.

doi: 10.1007/s43621-025-00920-8

35. Tahir Z, Haseeb M, Mahmood SA, Hassan NE, Dogar MM, Hassan SZ. From green to grey: assessing the impact of urbanization on land surface temperature and thermal comfort in Multan City. *Earth Syst Environ*. 2025;9(2):777-800.

doi: 10.1007/s41748-025-00598-y

36. Thangaraj K, Karthikeyan S, Kulandaisamy P, *et al*. Impacts of rapid urbanization on land surface temperature and environmental degradation in Madurai, India: a decadal analysis (2013-2023). *Theor Appl Climatol*. 2025;156(4):212.

doi: 10.1007/s00704-025-05442-x

37. Ullah S, Qiao X, Tariq A. Impact assessment of planned and unplanned urbanization on land surface temperature in Afghanistan using machine learning algorithms: a path toward sustainability. *Sci Rep*. 2025;15(1):3092.

doi: 10.1038/s41598-025-87234-x

38. Sandoval S, Escobar-Flores JG, Badar Munir M. Urbanization and its impacts on land surface temperature and sea surface temperature in a tourist region in Mexico from 1990 to 2020. *Remote Sens Appl Soc Environ*. 2023;32:101046.

doi: 10.1016/j.rsase.2023.101046

39. Ullah W, Ahmad K, Ullah S, *et al*. Analysis of the relationship among land surface temperature (LST), land use land cover (LULC), and normalized difference vegetation index (NDVI) with topographic elements in the lower Himalayan region. *Heliyon*. 2023;9(2):e13322.

doi: 10.1016/j.heliyon.2023.e13322

40. Rezapouraghdam H, Hidalgo-García D. Impacts of urbanization on land surface temperature and vegetation cover in a semi-arid city: the case of Maragheh. *Earth Syst Environ*. 2026;10(5):6217-6242.

doi: 10.1007/s41748-025-00951-1